RESEARCH ARTICLE • OPEN ACCESS

Discrete-Time Dynamics of Deposit-Loan Volumes Model with Repayment Rate: Standard and Non-Standard Approaches

Raqqasyi Rahmatullah Musafir and Meylita Sari

Volume 13, Issue 3, pp. 435–445, Dec. 2025

Received 28 October 2025, Revised 10 November 2025, Accepted 3 December 2025, Published 10 December 2025

To Cite this Article : R. R. Musafir and M. Sari,"Discrete-Time Dynamics of Deposit-Loan Volumes Model with Repayment Rate: Standard and Non-Standard Approaches", *Euler J. Ilm. Mat. Sains dan Teknol.*, vol. 13, no. 3, pp. 435–445, 2025, *https://doi.org/10.37905/euler.v13i3.35039*

JOURNAL INFO • EULER : JURNAL ILMIAH MATEMATIKA, SAINS DAN TEKNOLOGI

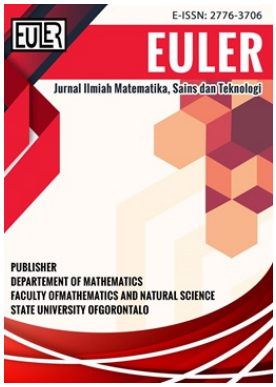

Homepage	:	http://ejurnal.ung.ac.id/index.php/euler/index
Journal Abbreviation	:	Euler J. Ilm. Mat. Sains dan Teknol.
Frequency	:	Three times a year
Publication Language	:	English (preferable), Indonesia
DOI	:	https://doi.org/10.37905/euler
Online ISSN	:	2776-3706
Publisher	:	Department of Mathematics, Universitas Negeri Gorontalo
Country	:	Indonesia
OAI Address	:	http://ejurnal.ung.ac.id/index.php/euler/oai
Google Scholar ID	:	QF_r-_gAAAAJ
Email	:	euler@ung.ac.id

JAMBURA JOURNAL • FIND OUR OTHER JOURNALS

Jambura Journal of Biomathematics

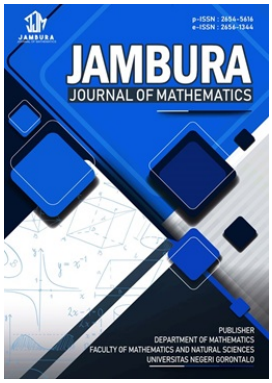

Jambura Journal of Mathematics

Jambura Journal of Mathematics Education

Jambura Journal of Probability and Statistics

Euler : Jurnal Ilmiah Matematika, Sains dan Teknologi, Volume 13, Issue 3, Pages 435–445, Dec. 2025 *https://doi.org/10.37905/euler.v13i3.35039*

Research Article

Discrete-Time Dynamics of Deposit-Loan Volumes Model with Repayment Rate: Standard and Non-Standard Approaches

Raqqasyi Rahmatullah Musafir[1,*], **Meylita Sari**[1]

[1]*Department of Mathematics, University of Brawijaya, Malang 65145, Indonesia*

ARTICLE HISTORY
Received 28 October 2025
Revised 10 November 2025
Accepted 3 December 2025
Published 10 December 2025

KEYWORDS
Forward Euler scheme
Non-standard finite difference
Stability analysis
Interest rate
Parameter estimation

ABSTRACT. *In the banking system, the repayment rate of loans, which is influenced by interest rates and non-performing loans, plays an important role in the bank's cash flow. In this paper, we propose a discrete model of deposit-loan volumes by considering the repayment rate. The proposed model involves the standard forward Euler discretization and the non-standard finite difference (NSFD) scheme. The numerical schemes of both models are explicitly defined. Both models have three fixed points, i.e., the transaction-free point, the loan-free point, and the active-transaction point. The transaction-free fixed point is unstable, while the other two are locally asymptotically stable under certain conditions. The stability of the Euler model's fixed point depends on the stepsize h. This indicates that the NSFD model is dynamically more consistent since it does not depend on h. Numerical simulations also confirm that the stability property of the NSFD model's fixed points does not depend on h. Meanwhile, the stability of the fixed points of Euler model depends on h. The simulations also show the Euler model undergoes the period-doubling and Neimark–Sacker bifurcations. This is indicated by changes in the stepsize that cause the convergence of the solution to shift into oscillations or even chaos. The chaotic condition is an undesired or even avoided situation in the banking sector. High and irregular fluctuations lead to the failure of policy control and liquidity projection. We also performed a case study using weekly loan data from September 2022 to March 2025 via parameter estimation. We use two performance metrics, i.e., the coefficient of determination (R^2) and the root mean square error (RMSE). Both models produce realistic parameter values and provide a good fit to the data trend, as observed visually and from R^2. Based on RMSE, the NSFD model performs better than the Euler model. Moreover, the larger the h, the better the performance. These results suggest the use of the NSFD model, which has better relevance and accuracy than the Euler model.*

1. Introduction

The dynamics of a country's economy cannot be separated from the financial cycle involving the banking sector. Banks play an important role in establishing monetary policies in order to maintain financial stability [1]. In addition, banks also support the government's fiscal policies to synergize in distributing and managing funds to the public. In performing their role, banks collect and manage funds from third parties with a surplus and then channel the funds to those in need in the form of loans [2]. In these loans, there exists an interest rate borne by the borrower as a compensation or service cost of the bank, which must be accumulated in the repayment [3]. The repayment funds from the borrower will enter the bank's cash flow to be managed further. However, repayment does not always proceed smoothly, such as the inability to repay according to the agreement, which is referred to as a non-performing loan [4]. This is very important to be considered in the cash flow of deposit-loan. The deposit-loan cycle is important to be studied in order to maintain the circulation of funds in the economy.

One of the ways to study the dynamics of deposit and loan volumes is through mathematical modeling. A deterministic compartmental mathematical model is able to capture the phenomena of the mechanisms among the variables involved [5]. Mathematical models have been widely used to describe various phenomena, such as epidemiology, industry, and ecology [5–7]. The predator-prey model is one of the models that describes the interaction between populations in an ecosystem [8]. One of the most popular models used is the Lotka–Volterra model, which assumes that the predator grows logistically and preys on the prey [9]. Through this model, Sumarti et al. [10] proposed a deposit–loan model with a Michaelis–Menten type loan rate and a reserve requirement ratio:

$$\begin{aligned} \frac{dD}{dt} &= rD\left(1-\frac{D}{K}\right) - \frac{\beta(1-s)DL}{1+(1-s)bD}, \\ \frac{dL}{dt} &= \frac{\beta(1-s)DL}{1+(1-s)bD} - \alpha L, \end{aligned} \tag{1}$$

where $D = D(t)$ and $L = L(t)$ are the time-dependent volumes of deposit and loan, respectively. The parameters involved are r, K, β, and α, which represent the deposit inflow rate, deposit fund capacity, loan rate, and non-performing loan, respectively. The parameters b and s denote the saturation proportion and the reserve requirement ratio, respectively.

*Corresponding Author.

Email : *rrmusafir@ub.ac.id* (R. R. Musafir)
Homepage : http://ejurnal.ung.ac.id/index.php/euler/index / E-ISSN : 2776-3706

The model of Sumarti et al. (1) was developed by Damayanti et al. [11] by involving personal and corporate loans. In addition, the model of Sumarti et al. (1) was also studied by Ramanda et al. [12] involving a stochastic model. However, the proposed model applies to a continuous time interval. In reality, the changes in deposit and loan volumes occur over discrete or countable time intervals. Moreover, the discrete version of the model exhibits more complex dynamics than the continuous one. This has motivated several researchers to discretize the continuous model [13, 14].

Discretization of the continuous model can be performed using the standard forward Euler approach. Several researchers who used this approach could not preserve dimensional consistency. Mickens [15] developed a discretization method using the non-standard finite difference (NSFD) approach. This approach performs better in maintaining dimensional consistency even with a larger stepsize [14, 16]. The discretization of the deposit–loan model has been performed by Pinto et al. [17] using the NSFD approach. The model studied by Pinto et al. is the discretization of model (1) with the assumption that the loan rate is bilinear. However, the saturation rate in model (1) represents a barrier to excessive deposits [11]. The Michaelis–Menten type rate in the model $\dfrac{\beta(1-s)DL}{1+(1-s)bD}$ also has the same meaning as the Holling type II rate $\dfrac{\beta(1-s)DL}{k+(1-s)D}$, with the half-saturation constant k through the transformation $\beta \to \dfrac{\beta}{k}$ and $b = \dfrac{1}{k}$.

The model (1) does not take into account the repayment rate, which is the source of the bank's profit from deposit–loan transactions. The profit depends on the interest rate and the proportion of non-performing loans [18, 19]. Here, we develop a discrete version of model (1) by modifying the Holling type II loan rate and adding the repayment rate from borrowers, which naturally involves the interest rate and the non-performing loan. The discrete models under study use two approaches, i.e., the forward Euler and the NSFD approaches.

2. Discrete-Time Deposit-Loan Model

Here, we develop the model proposed by Sumarti et al. [10] by adding the repayment rate from the loan and the saturated loan rate. Specifically, we consider two aspects. First, the cash outflow from the loan volume to the deposit volume is modeled bilinearly with the rate ρ, interest rate i, and the proportion of non-performing loans μ. Second, the Michaelis–Menten type loan rate is modified into a Holling type II rate with the half-saturation constant k. Thus, model (1) is extended into a continuous model with a repayment rate, which is given by

$$\begin{aligned}\frac{dD}{dt} &= rD\left(1-\frac{D}{K}\right) - \frac{\beta(1-s)DL}{k+(1-s)D} + \rho(1-\mu)(1+i)L,\\ \frac{dL}{dt} &= \frac{\beta(1-s)DL}{k+(1-s)D} - \alpha L - \rho(1-\mu)(1+i)L.\end{aligned} \tag{2}$$

We then perform the discretization of model (2) using both the standard (Euler) and non-standard methods. Let the observation interval of t be $[a,b]$, where $a,b \in \mathbb{R}_{\geq 0}$. The interval $[a,b]$ is divided into N equal subintervals, resulting in the intervals $[t_0,t_1),[t_1,t_2),\ldots,[t_{N-1},t_N]$. Using a discrete-time approach, the following standard and non-standard models are obtained.

2.1. Standard Euler Scheme

Here, the discrete model scheme is obtained using the forward Euler approach:

$$\frac{df}{dt} \to \frac{f_{n+1}-f_n}{h}$$

with $f_n = f(t_n)$ and $h = \Delta t = t_{n+1} - t_n$, where $n = 0,1,\ldots,N-1$. From this, we obtain the discrete model of the deposit–loan volumes using the standard approach:

$$\begin{aligned}D_{n+1} &= D_n + h\Big(rD_n\Big(1-\frac{D_n}{K}\Big) - \frac{\beta(1-s)D_nL_n}{k+(1-s)D_n} + \rho(1-\mu)\\ &\qquad (1+i)L_n\Big),\\ L_{n+1} &= L_n + h\left(\frac{\beta(1-s)D_nL_n}{k+(1-s)D_n} - \alpha L_n - \rho(1-\mu)(1+i)L_n\right),\end{aligned} \tag{3}$$

which is expressed in an explicit form.

2.2. Non-Standard Finite Difference Scheme

Basically, the non-standard finite difference scheme is performed by modifying the denominator function h into $\phi = O(h)$ or by approximating the nonlinear terms of the model using nonlocality [15]. Here, we retain the denominator function h as in the standard Euler scheme, but the nonlinear terms are approximated using nonlocality. The non-standard finite difference scheme can also preserve the non-negativity of the original model (2). The approximation of each term becomes:

$$\begin{aligned}&rD_n\left(1-\frac{D_n}{K}\right) \to rD_n\left(1-\frac{D_{n+1}}{K}\right),\\ &\frac{\beta(1-s)D_nL_n}{k+(1-s)D_n} \to \frac{\beta(1-s)D_{n+1}L_n}{k+(1-s)D_n},\\ &\rho(1-\mu)(1+i)L_n \to \rho(1-\mu)(1+i)L_{n+1},\\ &\alpha L_n \to \alpha L_{n+1}.\end{aligned}$$

Thus, the non-standard finite difference scheme of the discrete deposit–loan volume model is obtained as

$$\begin{aligned}D_{n+1} &= D_n + h\Big(rD_n\Big(1-\frac{D_{n+1}}{K}\Big) - \frac{\beta(1-s)D_{n+1}L_n}{k+(1-s)D_n}\\ &\qquad + \rho(1-\mu)(1+i)L_{n+1}\Big),\\ L_{n+1} &= L_n + h\Big(\frac{\beta(1-s)D_{n+1}L_n}{k+(1-s)D_n} - \alpha L_{n+1} - \rho(1-\mu)\\ &\qquad (1+i)L_{n+1}\Big).\end{aligned} \tag{4}$$

It can be observed that model (4) is in implicit form. If we denote $\Phi = 1 + h\alpha + h\rho(1-\mu)(1+i)$, then the explicit form of model (4) is given by

$$\begin{aligned}D_{n+1} &= \frac{K\left(k+(1-s)D_n\right)\left[\Phi D_n(1+hr) + h\rho(1-\mu)(1+i)L_n\right]}{\left(K+hrD_n\right)\left(k+(1-s)D_n\right)\Phi + K\left(1+h\alpha\right)h\beta(1-s)L_n},\\ L_{n+1} &= \frac{\left(k+(1-s)D_n\right)+h\beta(1-s)D_{n+1}}{\Phi\left(k+(1-s)D_n\right)}L_n.\end{aligned} \tag{5}$$

It can be observed that the non-standard scheme (5) preserves the non-negativity of the deposit volume D and the loan volume L. From this, the first difference between the standard Euler scheme and the non-standard finite difference scheme can be seen.

3. Fixed Point of Discrete-Time Model

The determination of the fixed points in an economic sense aims to evaluate the values of deposit and loan volumes when the corresponding system yields no change in each volume. In other words, the fixed points are determined through the analytical solution of the model when $D_{n+1} = D_n = D^*$ and $L_{n+1} = L_n = L^*$. Thus, both the standard model (3) and the non-standard model (5) have the same fixed points. The fixed points of the model are:

1. The transaction-free fixed point $F_0 = (0, 0)$, which always exists.
2. The loan-free fixed point $F_1 = (K, 0)$, which always exists.
3. The active-transaction fixed point $F_2 = (D_2, L_2)$, where $D_2 = \frac{(\alpha+\rho(1-\mu)(1+i))k}{(1-s)(\beta-(\alpha+\rho(1-\mu)(1+i)))}$ and $L_2 = \frac{rD_2}{\alpha}\left(1 - \frac{D_2}{K}\right)$. This fixed point exists if $0 < \frac{(\alpha+\rho(1-\mu)(1+i))k}{(1-s)(\beta-(\alpha+\rho(1-\mu)(1+i)))} < K$.

4. Stability of Fixed Points

Among the three obtained fixed points, the active-transaction fixed point F_2 is expected to exist, and the model solution is expected to converge to this point in order to achieve a stable economic condition. Here, the stability of the fixed point is analyzed to obtain information regarding whether the fixed point is stable or not. If the fixed point is stable, it indicates that the solutions in the neighborhood of the fixed point will converge to it as time progresses. The stability of each fixed point for the respective schemes is analyzed locally through the linearization of the proposed numerical schemes [20].

4.1. Stability Analysis of Standard Euler Scheme

Here, we analyze the local stability of each fixed point through the linearization of model (3) around the fixed point. Suppose that (D^*, L^*) is a fixed point of model (3). The Jacobian matrix around the point (D^*, L^*) can be obtained as

$$H_{(D^*,L^*)} = \begin{bmatrix} h_{11} & h_{12} \\ h_{21} & h_{22} \end{bmatrix},$$

where,

$$\begin{aligned}
h_{11} &= 1 + h\left(r - \frac{2rD^*}{K} - \frac{\beta(1-s)kL^*}{(k+(1-s)D^*)^2}\right),\\
h_{12} &= h\left(-\frac{\beta(1-s)D^*}{k+(1-s)D^*} + \rho(1-\mu)(1+i)\right),\\
h_{21} &= h\left(\frac{\beta(1-s)kL^*}{(k+(1-s)D^*)^2}\right),\\
h_{22} &= 1 + h\left(\frac{\beta(1-s)D^*}{k+(1-s)D^*} - \alpha - \rho(1-\mu)(1+i)\right).
\end{aligned}$$

The stability of each fixed point is given by the following theorems.

Theorem 1. *The fixed point $F_0 = (0, 0)$ is unstable. Meanwhile, the fixed point F_1 is locally asymptotically stable if and only if the following two conditions hold:*

1. $0 < hr < 1$, *and*
2. $0 < h\left(\frac{\alpha+\rho(1-\mu)(1+i)-\beta(1-s)K}{k+(1-s)K}\right) < 2$.

Proof. First, we observe the stability of the fixed point F_0. The Jacobian matrix evaluated at the point $(0, 0)$ is an upper triangular matrix and has the characteristic equation:

$$(1 + hr - \lambda)\left(1 - h(\alpha + \rho(1-\mu)(1+i)) - \lambda\right) = 0.$$

It is clear that one of the eigenvalues is $\lambda = 1 + hr > 1$, hence the point $(0, 0)$ is unstable.

Next, we observe the characteristic equation of the Jacobian matrix $H_{(K,0)}$, which is also a triangular matrix, i.e.,:

$$(1 - hr - \lambda)\left(1+h\Big(\frac{\beta(1-s)K}{k+(1-s)K} - \alpha - \rho(1-\mu)(1+i)\Big) - \lambda\right) = 0.$$

The eigenvalues can be obtained as $\lambda_1 = 1 - hr$ and $\lambda_2 = 1 + h\left(\frac{\beta(1-s)K}{k+(1-s)K} - \alpha - \rho(1-\mu)(1+i)\right)$. Each eigenvalue satisfies $|\lambda_j| < 1$ for $j = 1, 2$ if and only if $0 < hr < 2$ and $0 < h\left(\frac{\alpha+\rho(1-\mu)(1+i)-\beta(1-s)K}{k+(1-s)K}\right) < 2$. Under these two conditions, the fixed point F_1 is locally asymptotically stable. The proof is complete. □

Theorem 2. *Suppose that $\beta - (\alpha + \rho(1-\mu)(1+i)) > 0$ and $D_2 < K$, such that the fixed point F_2 exists. The point F_2 is locally asymptotically stable if all the following conditions hold:*

1. $4+2h\left(r - \frac{2rD_2}{K} - \frac{\beta(1-s)kL_2}{(k+(1-s)D_2)^2}\right)+h^2\frac{\alpha\beta(1-s)kL_2}{(k+(1-s)D_2)^2} > 0$, *and*
2. $0 < hr\left(\frac{2D_2}{K} - 1\right) + (h-1)h\frac{\alpha\beta(1-s)kL_2}{(k+(1-s)D_2)^2} < 2$.

Proof. Assume that the fixed point F_2 exists, that is, $\beta - (\alpha + \rho(1-\mu)(1+i)) > 0$ and $D_2 < K$. The characteristic equation of the Jacobian matrix around F_2 is

$$P_1(\lambda) = \lambda^2 + A_1\lambda + A_2 = 0,$$

where

$$\begin{aligned}
A_1 &= -\Big(2 + h\Big(r - \frac{2rD_2}{K} - \frac{\beta(1-s)kL_2}{(k+(1-s)D_2)^2}\Big)\Big),\\
A_2 &= 1 + h\Big(r - \frac{2rD_2}{K} - \frac{\beta(1-s)kL_2}{(k+(1-s)D_2)^2}\Big)\\
&\quad + h^2\frac{\alpha\beta(1-s)kL_2}{\Big(k+(1-s)D_2\Big)^2}.
\end{aligned}$$

First, we observe the following values of $P_1(1)$ and $P_1(-1)$:

$$\begin{aligned}
P(1) &= 1 + A_1 + A_2 = h^2\frac{\alpha\beta(1-s)kL_2}{(k+(1-s)D_2)^2} > 0,\\
P(-1) &= 1 - A_1 + A_2
\end{aligned}$$

$$= 4 + 2h\left(r - \frac{2rD_2}{K} - \frac{\beta(1-s)kL_2}{(k+(1-s)D_2)^2}\right) + h^2\frac{\alpha\beta(1-s)kL_2}{(k+(1-s)D_2)^2}.$$

It can also be observed that

$$A_2 = 1 + h\left(r - \frac{2rD_2}{K}\right) + (h-1)h\frac{\alpha\beta(1-s)kL_2}{(k+(1-s)D_2)^2}.$$

According to the Jury Conditions [21], the point F_2 is locally asymptotically stable if $P(-1) > 0$ and $|A_2| < 1$. Hence, $|A_2| < 1$ if

$$0 < hr\left(\frac{2D_2}{K} - 1\right) + (h-1)h\frac{\alpha\beta(1-s)kL_2}{(k+(1-s)D_2)^2} < 2.$$

The proof is complete. □

4.2. *Stability Analysis of Non-Standard Finite Difference Scheme*

The stability analysis of the fixed points for the non-standard scheme (5) uses the same mechanism as before. Suppose that (D^*, L^*) is an existing fixed point of model (5). Let

$$\begin{aligned}
G_0 &= K\left(k+(1-s)D^*\right)\left[\Phi D^*(1+hr) + h\rho(1-\mu)(1+i)L^*\right],\\
G_1 &= K(1-s)\left[\Phi D^*(1+hr) + h\rho(1-\mu)(1+i)L^*\right] + \Phi(1+hr)\\
G_2 &= \left(K+hrD^*\right)\left(k+(1-s)D^*\right)\Phi + K(1+h\alpha)h\beta(1-s)L^*,\\
G_3 &= \left(hr(k+(1-s)D^*) + (1-s)(K+hrD^*)\right)\Phi.
\end{aligned}$$

The Jacobian matrix evaluated at the point (D^*, L^*) is

$$J_{(D^*,L^*)} = \begin{bmatrix} J_{11} & J_{12} \\ J_{21} & J_{22} \end{bmatrix},$$

where

$$\begin{aligned}
J_{11} &= \frac{G_1G_2 - G_3G_0}{G_2^2},\\
J_{12} &= \frac{J_{12}^a}{G_2^2},\\
J_{12}^a &= h\rho(1-\mu)(1+i)K\left(k+(1-s)D^*\right)G_2\\
&\quad - K(1+h\alpha)h\beta(1-s)G_0,\\
J_{21} &= \frac{J_{11}k + (J_{11}-1)(1-s)D^*}{\Phi(k+(1-s)D^*)^2}h\beta(1-s)L^*,\\
J_{22} &= \frac{k+(1+h\beta)(1-s)D^*}{\Phi\left(k+(1-s)D^*\right)}.
\end{aligned}$$

The stability of each fixed point of model (5) is given by the following theorems.

Theorem 3. *The fixed point F_0 is always unstable.*

Proof. For the point F_0, we obtain $G_0 = 0$, $G_1 = \Phi(1+hr)Kk$, $G_2 = Kk\Phi$, and $G_3 = (hrk + (1-s)K)\Phi$. The Jacobian matrix evaluated at P_0 is

$$J_{(0,0)} = \begin{bmatrix} (1+hr) & \frac{h\rho(1-\mu)(1+i)}{\Phi(1+hr)} \\ 0 & \frac{1}{\Phi} \end{bmatrix}.$$

The eigenvalues of the matrix $J_{(0,0)}$ are $\lambda_1 = 1+hr$ and $\lambda_2 = \frac{1}{\Phi}$. It is clear that the point F_0 is unstable since $\lambda_1 > 1$. □

Theorem 4. *If $\beta(1-s)K < \left(k+(1-s)K\right)\left(\alpha+\rho(1-\mu)(1+i)\right)$, then the fixed point F_1 is locally asymptotically stable.*

Proof. Since $F_1 = (K, 0)$, we have $G_0 = K^2(k+(1-s)K)\Phi(1+hr)$, $G_1 = \Phi(1+hr)Kk + 2\Phi K^2(1+hr)(1-s)$, $G_2 = K(1+hr)(k+(1-s)K)\Phi$, and $G_3 = (hrk+2hr(1-s)K+(1-s)K)\Phi$. The Jacobian matrix evaluated at P_1 is

$$J_{(K,0)} = \begin{bmatrix} \frac{1}{1+hr} & \frac{h\rho(1-\mu)(1+i)(k+(1-s)K) - K(1+h\alpha)h\beta(1-s)}{(1+hr)(k+(1-s)K)\Phi} \\ 0 & \frac{k+(1-s)K+h\beta(1-s)K}{\Phi(k+(1-s)K)} \end{bmatrix}.$$

It is straightforward to obtain the eigenvalues of $J_{(K,0)}$, i.e., $\lambda_1 = \frac{1}{1+hr}$ and $\lambda_2 = \frac{k+(1-s)K+h\beta(1-s)K}{\Phi(k+(1-s)K)}$. It can be observed that $0 < \lambda_1 < 1$ and $\lambda_2 > 0$. Each eigenvalue satisfies $|\lambda_j| < 1$ for $j = 1, 2$ if $\beta(1-s)K < \left(k+(1-s)K\right)\left(\alpha+\rho(1-\mu)(1+i)\right)$. Under this condition, the fixed point F_1 is locally asymptotically stable. □

Theorem 5. *Suppose that the fixed point F_2 exists under the condition $0 < \frac{(\alpha+\rho(1-\mu)(1+i))k}{(1-s)(\beta-(\alpha+\rho(1-\mu)(1+i)))} < K$. The fixed point F_2 is locally asymptotically stable if all the following criteria are satisfied.*

1. $1 - \left(J_{11}^{(2)} + J_{22}^{(2)}\right) + J_{11}^{(2)}J_{22}^{(2)} - J_{12}^{(2)}J_{21}^{(2)} > 0$
2. $1 + \left(J_{11}^{(2)} + J_{22}^{(2)}\right) + J_{11}^{(2)}J_{22}^{(2)} - J_{12}^{(2)}J_{21}^{(2)} > 0$
3. $\left|J_{11}^{(2)}J_{22}^{(2)} - J_{12}^{(2)}J_{21}^{(2)}\right| < 1$

where $J_{11}^{(2)}$, $J_{22}^{(2)}$, $J_{12}^{(2)}$, and $J_{21}^{(2)}$ are provided in the proof.

Proof. Assume that $0 < \frac{(\alpha+\rho(1-\mu)(1+i))k}{(1-s)(\beta-(\alpha+\rho(1-\mu)(1+i)))} < K$ so that the active-transaction fixed point $F_2 = (D_2, L_2)$ exists, where $D_2 = \frac{(\alpha+\rho(1-\mu)(1+i))k}{(1-s)(\beta-(\alpha+\rho(1-\mu)(1+i)))}$ and $L_2 = \frac{rD_2}{\alpha}\left(1 - \frac{D_2}{K}\right)$. The characteristic equation of the Jacobian matrix $J_{(D_2,L_2)}$ is

$$P_2(\lambda) = \lambda^2 - \left(J_{11}^{(2)} + J_{22}^{(2)}\right)\lambda + J_{11}^{(2)}J_{22}^{(2)} - J_{12}^{(2)}J_{21}^{(2)} = 0,$$

where

$$\begin{aligned}
J_{11}^{(2)} &= \frac{G_1^*G_2^* - G_3^*G_0^*}{(G_2^*)^2},\\
J_{12}^{(2)} &= \frac{J_{12}^{(2)a}}{(G_2^*)^2},\\
J_{12}^{(2)a} &= h\rho(1-\mu)(1+i)K\left(k+(1-s)D_2\right)G_2^*\\
&\quad - K(1+h\alpha)h\beta(1-s)G_0^*,\\
J_{21}^{(2)} &= \frac{J_{11}^{(2)}k + (J_{11}^{(2)}-1)(1-s)D_2}{\Phi(k+(1-s)D_2)^2}h\beta(1-s)L_2,\\
J_{22}^{(2)} &= \frac{k+(1+h\beta)(1-s)D_2}{\Phi\left(k+(1-s)D_2\right)},\\
G_0^* &= K\left(k+(1-s)D_2\right)\left[\Phi D_2(1+hr) + h\rho(1-\mu)(1+i)L_2\right],\\
G_1^* &= K(1-s)\left[\Phi D_2(1+hr) + h\rho(1-\mu)(1+i)L_2\right]\\
&\quad + \Phi(1+hr)K\left(k+(1-s)D_2\right),
\end{aligned}$$

Table 1. Parameter values in numerical simulation

	r	K	β	s	k	ρ	μ	i	α
First Simulation	0.1	100	0.01	0.02	10	0.02	0.05	0.06	0.005
Second Simulation	0.1	20	0.9	0.02	50	0.0002	0.5	0.6	0.05

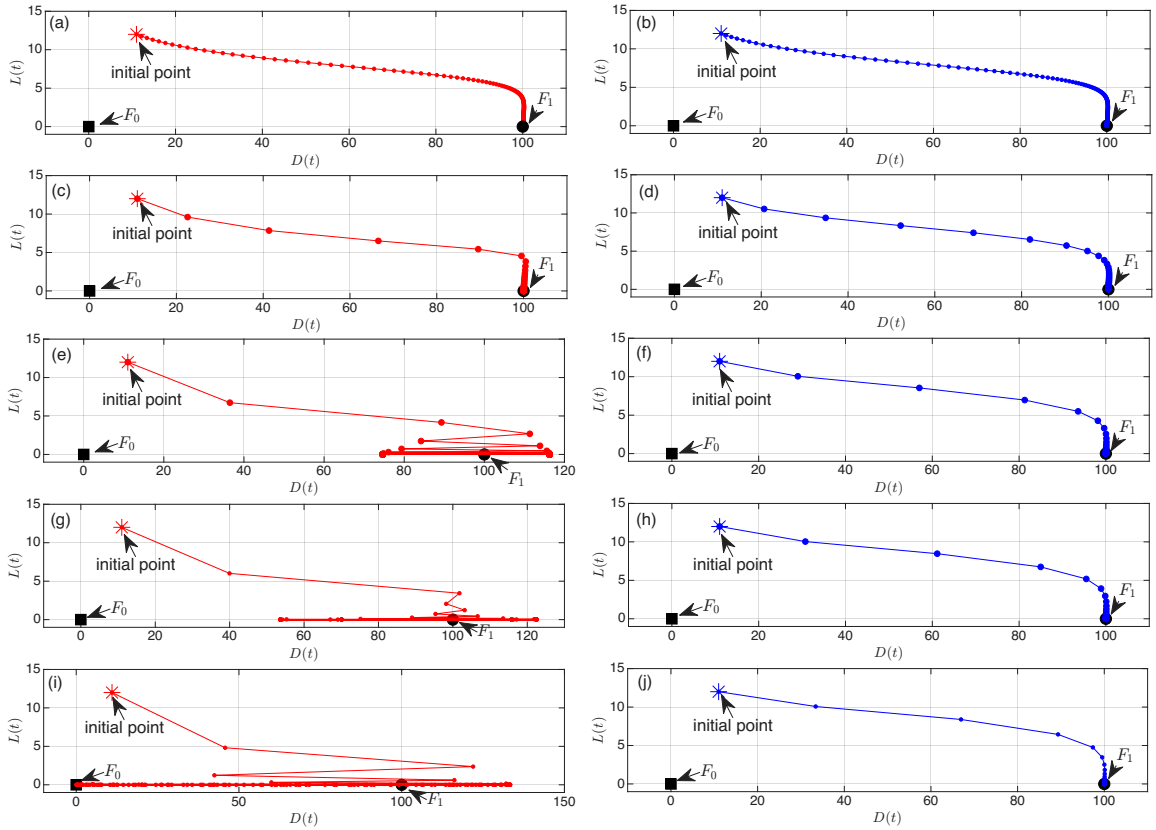

Figure 1. Trajectories of the Euler and NSFD schemes for several stepsizes: (a) Euler $h = 1$, (b) NSFD $h = 1$, (c) Euler $h = 10$, (d) NSFD $h = 10$, (e) Euler $h = 22$, (f) NSFD $h = 22$, (g) Euler $h = 25$, (h) NSFD $h = 25$, (i) Euler $h = 30$, (j) NSFD $h = 30$.

$G_2^* = (K + hrD_2)\,(k + (1-s)D_2)\,\Phi + K(1+h\alpha)h\beta(1-s)L_2,$
$G_3^* = (hr(k + (1-s)D_2) + (1-s)(K + hrD_2))\,\Phi.$

Due to the complexity of the terms in the characteristic equation, the fixed point F_2 is asymptotically stable if the Jury criteria [21] are satisfied, i.e., $P_2(1) > 0$, $P_2(-1) > 0$, and $|P_2(0)| < 1$. The proof is complete. □

5. Numerical Simulation

In this section, we perform numerical simulations to observe the behavior of the solutions of models (3) and (5). The parameter selection for the simulation is based on experimental results such that the conditions for the stability of each fixed point are satisfied. Thus, the stability of the fixed points can be confirmed, and the existing phenomena can be elaborated. In the first simulation, we use the parameter values $r = 0.1$, $K = 100$, $\beta = 0.01$, $s = 0.02$, $k = 10$, $\rho = 0.02$, $\mu = 0.05$, $i = 0.06$, and $\alpha = 0.005$, as listed in Table 1. These parameter values yield $\frac{\beta(1-s)K}{(k+(1-s)K)(\alpha+\rho(1-\mu)(1+i))} = 0.3609 < 1$, which satisfies the sufficient condition of Theorem 4. This indicates that the solution of model (5) converges to the fixed point $F_1 = (20, 0)$ for any h. Meanwhile, the convergence of the solution of model (3) depends on the stepsize h. Here, we use the initial point $(11, 12)$, resulting in the solutions illustrated in Figure 1. It can be observed that both solutions for $h = 1$, depicted in Figures 1(a) and (b), converge to the point F_1. Similarly, the solutions for $h = 10$, shown in Figures 1(c) and (d), also converge to F_1. When $h = 22$, the Euler model (3) exhibits oscillations at several points, as shown in Figure 1(e), while Figure 1(f) shows that the NSFD model (5) converges to the fixed point F_1. When the stepsize is increased to $h = 25$ and $h = 30$, the Euler model (3) exhibits oscillations at more points, while the NSFD model (5) continues to converge to F_1. This indicates that the NSFD model (5) is more consistent, regardless of the stepsize h. This consistency can also be identified from the stability condition of fixed point F_1, where the Euler model depends on the stepsize h, while the NSFD model does not. Hence, changes in the stepsize may affect the eigenvalues of the matrix $H_{(K,0)}$ at the stability of the fixed point F_1, leading to absolute eigenvalues greater than unity. This indicates that the Euler model may generate oscillations involving two or more points.

The solution of the Euler model (3) for $h = 22, 25, 30$ is further examined due to the indication of oscillations through the time-series trajectory, as illustrated in Figure 2. It can be observed that the solution for $h = 22$, shown in Figure 2(a), oscillates at two points, indicating a 2-period behavior. When

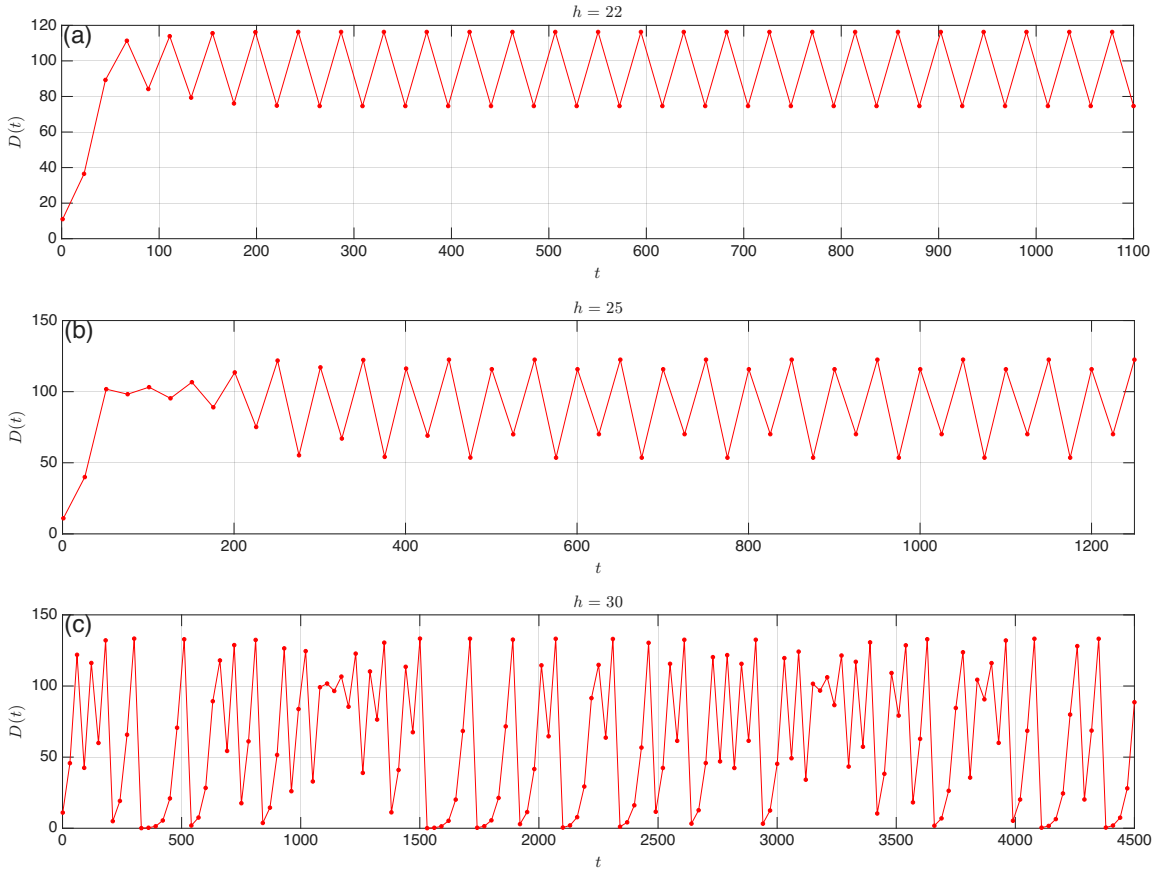

Figure 2. Time series for $D(t)$ that capture period-doubling and chaos for several h: (a) $h = 22$, (b) $h = 25$, (c) $h = 30$.

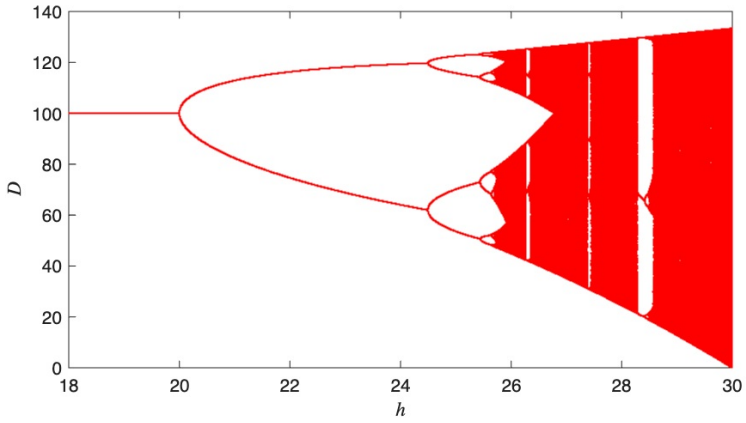

Figure 3. Diagram of period-doubling bifurcation.

$h = 25$, the solution shown in Figure 2(b) oscillates at four points, corresponding to a 4-period behavior. When the stepsize is increased to $h = 30$, chaos occurs, as depicted in Figure 2(c). Furthermore, we perform a bifurcation diagram simulation for $h \in [18, 30]$, which is illustrated in Figure 3. It can be seen that the model solution initially converges to the fixed point $(K, 0)$, then oscillates with period-2 ($24.49 < h < 25.44$), period-4 ($25.45 < h < 25.64$), and period-8 ($25.65 < h < 25.68$), and eventually becomes chaotic as h increases. This indicates that the model undergoes a period-doubling bifurcation [22].

From an economic perspective, the stable condition at the fixed point F_1 is undesirable since it implies that there will be no loans from customers in the future. For the Euler model (3), the periodic condition for the deposit volume and the zero condition for the loan volume are also undesirable. Moreover, the chaotic condition of the deposit volume becomes irrelevant for Indonesian banks, which are relatively stable. The chaotic behavior also indicates high volatility, making the deposit volume difficult to control.

The next simulation is performed to confirm the stability of the fixed point F_2. The parameter values used are $r = 0.1$, $K = 20$, $\beta = 0.9$, $s = 0.02$, $k = 50$, $\rho = 0.0002$, $\mu = 0.5$, $i = 0.6$, and $\alpha = 0.05$, as listed in Table 1. There exist three fixed points, i.e., $F_0 = (0, 0)$, $F_1 = (20, 0)$, and $F_2 = (3.011, 5.116)$.

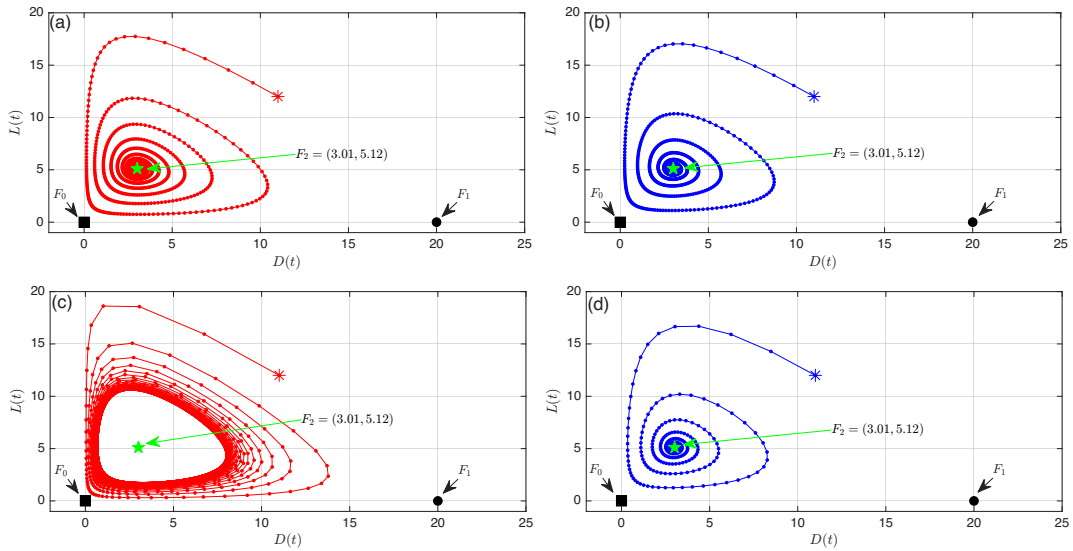

Figure 4. Trajectories of the Euler and NSFD schemes for several stepsizes: (a) Euler $h = 1$, (b) NSFD $h = 1$, (c) Euler $h = 3$, (d) NSFD $h = 3$.

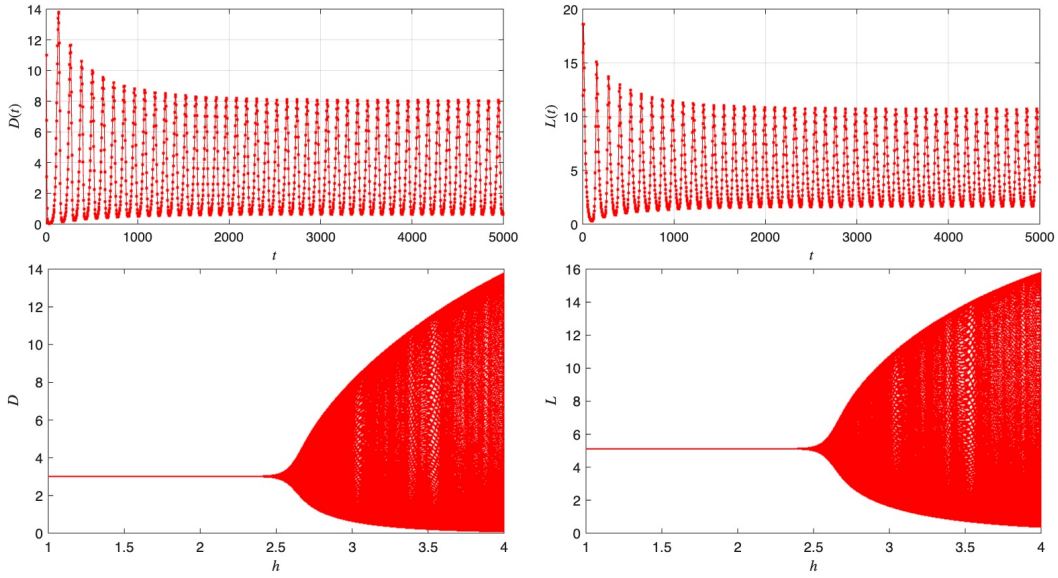

Figure 5. Diagram of Neimark–Sacker bifurcation.

For these parameter values and $h = 1$, it can be observed that the fixed point F_2 is asymptotically stable, as shown in Figures 4(a) and 4(b). When the stepsize is increased to $h = 3$, the solution of the NSFD model converges to the fixed point F_2, while the solution of the Euler model exhibits a periodic cycle. This indicates that the NSFD model is more consistent with respect to the stability of the fixed point and is not affected by the stepsize. The dynamical consistency of the NSFD model can be observed through the analytical results, which show that the stability condition of the fixed point does not depend on the stepsize. Thus, increasing the stepsize does not affect the stability of the fixed point of NSFD model. Meanwhile, the stability of the fixed point in the Euler model depends on the stepsize h, which means that significant changes in h can alter the fixed stability and may trigger the appearance of periodic cycles.

The phenomenon of periodic cycles in the Euler model can be further elaborated via time-series trajectories and bifurcation diagrams. The trajectory depicted in Figure 5 shows that the solution exhibits periodic cycles for sufficiently large time intervals t. The bifurcation diagram illustrated in Figure 5 shows that the solution of the Euler model converges to the fixed point F_2 when $h = 2$. If $h > 2.5$, the solution of the model exhibits periodic cycles. This indicates that the model undergoes a Neimark–Sacker bifurcation [22].

From an economic perspective, the second simulation condition is the desired one. The condition in which the model solution converges to the point F_2 with damped oscillations is desirable from a banking perspective, since continuous lending and borrowing occur throughout the time period, allowing customers to borrow money from banks through credit to drive the microeconomic sector. On the other hand, banks earn profits from repayments that involve interest costs, which constitute one

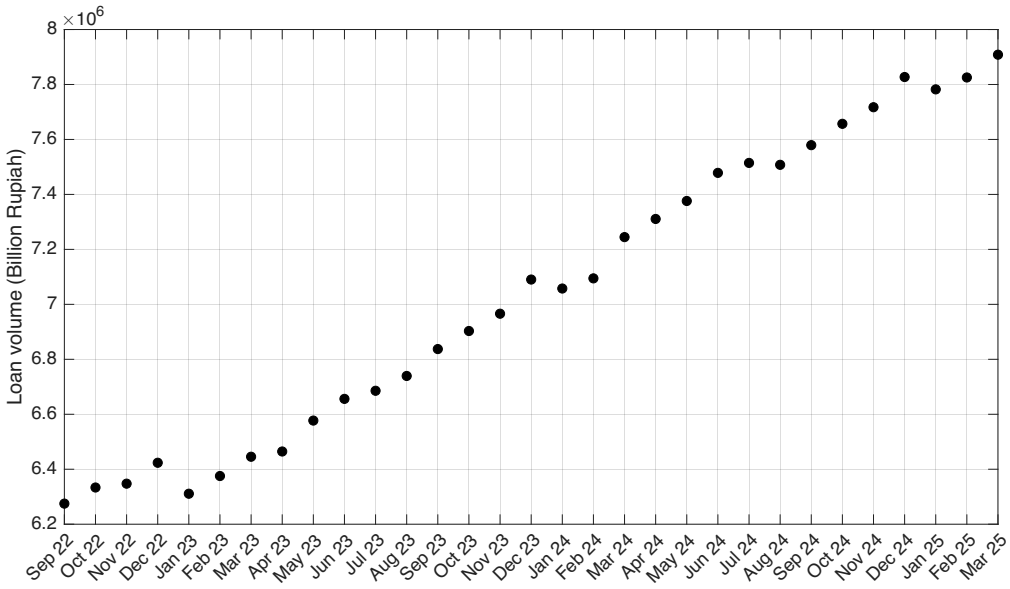

Figure 6. Weekly loan data of commercial banks in Indonesia from September 2022 to March 2025.

Table 2. Initial guess, lower bound (LB), and upper bound (UB) in parameter estimation

	r	K	β	s	k	ρ	μ	i	α
Initial	0.1	10^7	0.05	0.1	100	10^{-4}	0.01	0.5	0.005
LB	0	1	0	0	10	0	0	0	0
UB	1	10^{10}	1	1	$7 \cdot 10^8$	1	0.2	0.1	0.2

of the sources of bank profit. It can also be observed that the second simulation shows a Neimark–Sacker bifurcation for the Euler model. This condition is also desirable from an economic standpoint, where the deposit volume and loan volume exhibit continuous oscillations without reaching a stable fixed value of deposit and loan volumes.

6. Implementation to Loan Data

In this section, we perform fitting of the standard Euler discrete model (3) and the non-standard model (5) to the loan data for several stepsizes h. The loan data are collected from the open-access page of the Financial Services Authority (Otoritas Jasa Keuangan, OJK): https://ojk.go.id [23]. The collected data consist of weekly data from September 2022 to March 2025, as illustrated in Figure 6. It can be observed that the 31 loan data points exhibit a relatively increasing trend over time.

The model fitting is performed via parameter estimation using a non-heuristic method, i.e., nonlinear least squares. The estimation method is supported by the built-in MATLAB function *lsqcurvefit*, which provides model fitting to the data with initial guesses and parameter ranges as inputs. The initial guesses and ranges of each estimated parameter are given in Table 2. The initial value of both models is $(30000000, 6274901)$, where the initial loan value is taken from the first data point.

In this estimation, we compare the standard discrete model (3) and the non-standard model (5) based on the coefficient of determination (R^2) and the root mean square error (RMSE). The coefficient of determination of the model with respect to the data is given by the formula:

$$R^2 = 1 - \frac{\sum_{j=1}^{31} \left(L_{(data)}(t_j) - L(t_j)\right)^2}{\sum_{j=1}^{31} \left(L_{(data)}(t_j) - \bar{L}\right)^2},$$

where t_i denotes the i-th time point of the data, $L_{(data)}(t_i)$ is the loan data at t_i, $L(t_i)$ is the loan solution at t_i obtained from the model, and $\bar{L}$ is the mean of the data. Meanwhile, the RMSE is given by the formula

$$\text{RMSE} = \sqrt{\frac{\sum_{j=1}^{31} \left(L_{(data)}(t_j) - L(t_i)\right)^2}{31}}.$$

Both models (3) and (5) are compared based on several stepsizes, i.e., 0.01, 0.1, and 1.

The parameter estimation of the Euler model (3) and the NSFD model (5) with respect to the data yields the parameter values listed in Table 3. It can be observed that the deposit growth rate of the Euler model is higher than that of the NSFD model. The proportion of NPL in the NSFD model is much smaller than that in the Euler model, while the reserve requirement ratio of both models is relatively similar. In terms of the interest rate, the estimation results show that the interest rate in the Euler model ranges from 3% to 5%, whereas the NSFD model produces an interest rate between 0.65% and 9%. This indicates that both models still produce realistic values, except for the reserve requirement ratio in the NSFD model.

For the stepsize $h = 0.01$, the solutions of the Euler and NSFD models depicted in Figure 7 show that both models produce relatively similar estimations, and it is not possible to determine visually which one performs better. The estimations of

Table 3. Estimated parameter values of standard and non-standard models (3)–(5).

	Standard Model			Non-Standard Model		
	$h = 0.01$	$h = 0.1$	$h = 1$	$h = 0.01$	$h = 0.1$	$h = 1$
r	0.5094	0.5014	0.5430	0.3093	0.0289	0.0069
K	$6.67 \cdot 10^8$	$2.13 \cdot 10^8$	$1.82 \cdot 10^8$	$6.78 \cdot 10^9$	$3.90 \cdot 10^6$	$2.23 \cdot 10^6$
β	0.0414	0.0473	0.0312	0.8518	0.9003	0.4476
s	0.1280	0.1131	0.0869	0.1230	0.0627	0.0715
k	$7.65 \cdot 10^6$	$7.53 \cdot 10^6$	$1.11 \cdot 10^7$	$3.21 \cdot 10^5$	$9.25 \cdot 10^3$	$1.74 \cdot 10^5$
ρ	0.0240	0.0256	0.0154	0.6444	0.7813	0.3553
μ	0.0430	0.0159	0.0795	$6.97 \cdot 10^{-7}$	$1.31 \cdot 10^{-7}$	$2.86 \cdot 10^{-9}$
i	0.0415	0.0485	0.0318	0.0826	0.0894	0.0688
α	0.0083	0.0104	0.0060	0.1466	0.0317	0.0255

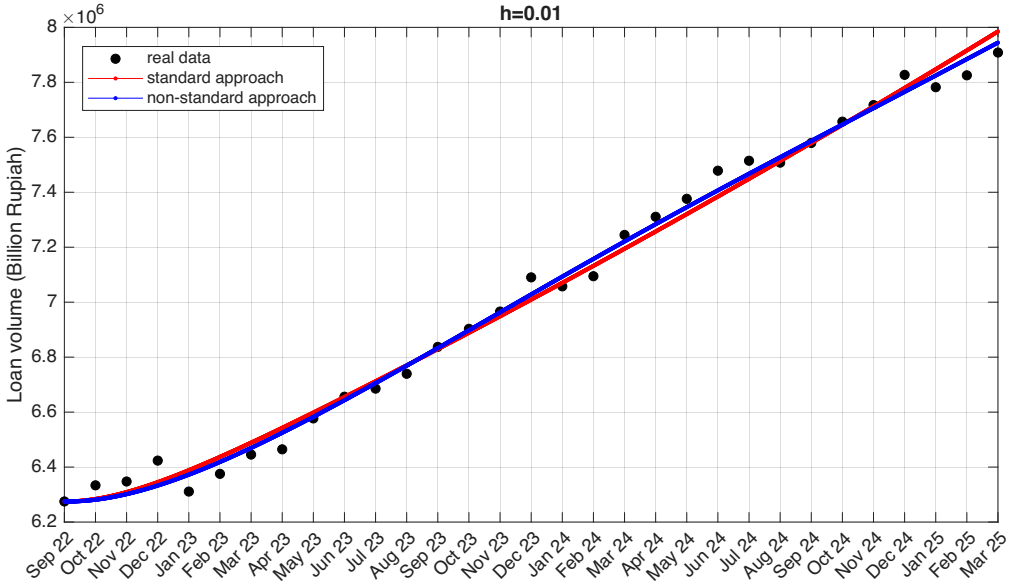

Figure 7. Fitted curve of model (3) and (5) in calibrating loan data for $h = 0.01$.

both models are able to capture the upward trend of the data until the end of the period. This illustrates that both models provide good results for small stepsizes.

For the stepsize $h = 0.1$, the difference between the two estimation results depicted in Figure 8 begins to appear. It can be observed in the third and fourth quarters that the estimated solution of the NSFD model provides a better approximation than that of the Euler model. Moreover, the fitting of the NSFD model for $h = 0.1$ is better than that for $h = 0.01$. This indicates that the stepsize h relatively affects the fitting results of the model.

For the stepsize increased to $h = 1$, so that the data and time have the same time scale, the estimation results are illustrated in Figure 9. The estimation of the NSFD model again provides a better approximation to the data compared to the Euler model. This is more apparent when observing the distance between the estimated results and the data at the same time points. In general, the NSFD model has a closer distance to the data compared to the Euler model. From the three stepsize scenarios, the NSFD model produces a better fitting than the Euler model.

To evaluate the performance of each fitting, we calculate R^2 and RMSE, which are listed in Table 4 and Table 5, respectively. The determination coefficient of the Euler model is around 0.991 for each h. Meanwhile, the determination coefficient of the NSFD model increases as the stepsize h becomes larger, i.e., from 0.994 to 0.995. From the determination coefficients, it can be observed that both models provide good estimations, i.e., greater than 99%.

Table 4. Determination coefficient (R^2) of model calibration.

	$h = 0.01$	$h = 0.1$	$h = 1$
Standard model (3)	0.991	0.991	0.991
Non-standard model (5)	0.994	0.994	0.995

Table 5. Root mean square error (RMSE) of model calibration ($\times 10^3$).

	$h = 0.01$	$h = 0.1$	$h = 1$
Standard model (3)	9.345	9.343	9.277
Non-standard model (5)	7.636	7.023	6.865

From the RMSE values listed in Table 5, the Euler model has an RMSE greater than $9 \cdot 10^3$, while the NSFD model has an RMSE below that for the same stepsize h. This indicates that the calibration performance of the NSFD model is better than that of the Euler model for each corresponding stepsize. Moreover, the larger the stepsize, the better the calibration performance of both models. The NSFD model exhibits a significant performance improvement from $h = 0.01$ to $h = 0.1$, with RMSE decreasing

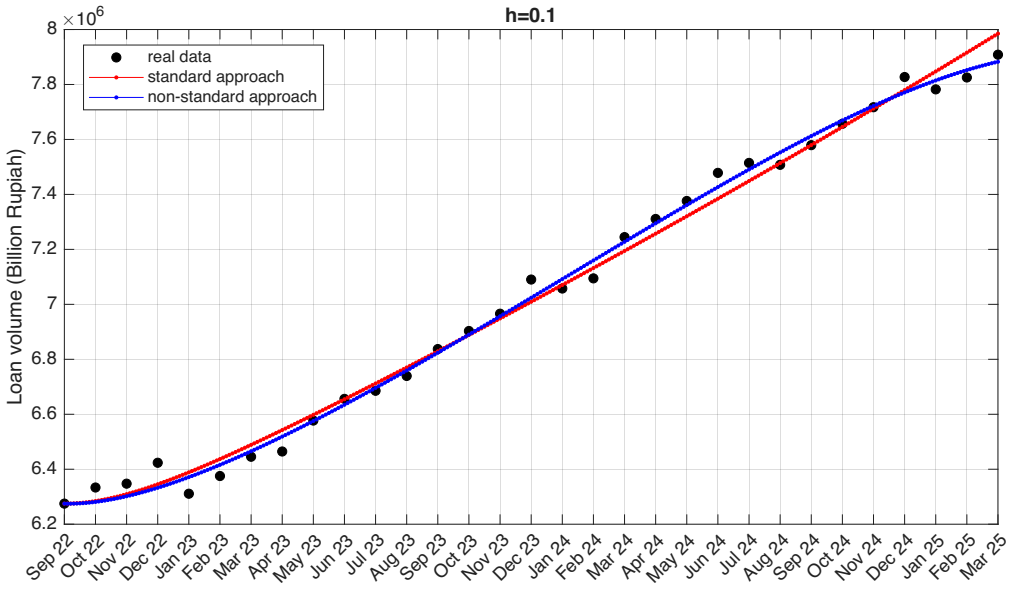

Figure 8. Fitted curve of model (3) and (5) in calibrating loan data for $h = 0.1$.

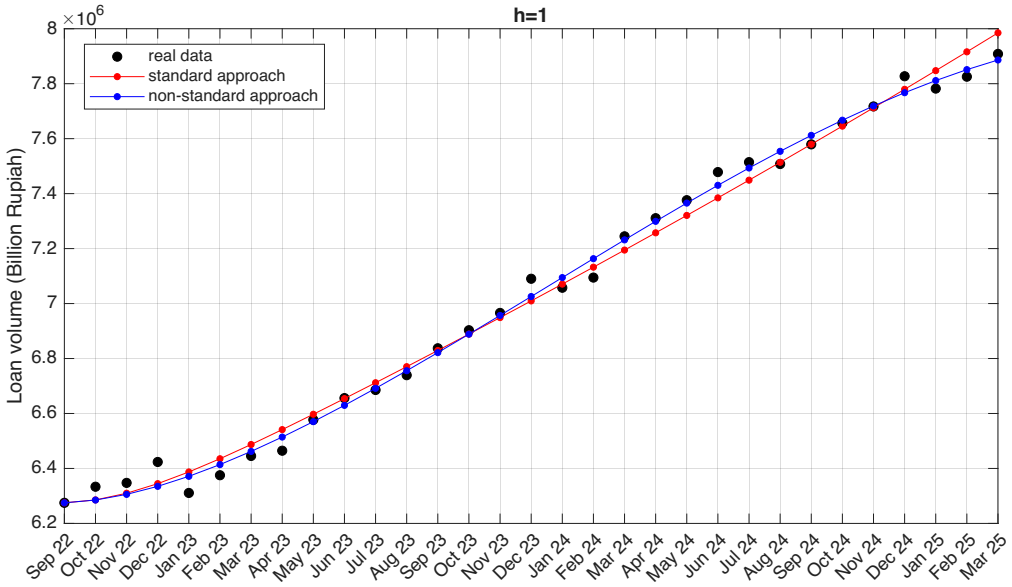

Figure 9. Fitted curve of model (3) and (5) in calibrating loan data for $h = 1$.

from $7.636 \cdot 10^3$ to $7.023 \cdot 10^3$, respectively. This confirms the visual results that show a significant difference in calibration performance between $h = 0.01$ and $h = 0.1$.

7. Conclusion

A discrete model of deposit–loan volumes with a repayment rate has been proposed in the explicit form of both the standard forward Euler and the non-standard finite difference (NSFD) schemes. The fixed points of the model have also been determined, i.e., the transaction-free point, the loan-free point, and the active-transaction point. The local stability of each fixed point has been analyzed. The transaction-free point is never stable, while the loan-free and active-transaction points are asymptotically stable under certain conditions. The difference between the stability conditions of the Euler and NSFD models lies in their dependence on the stepsize h, where each sufficient stability condition of the Euler model depends on h. Numerical simulations have confirmed this and concluded that the NSFD model is dynamically more consistent, whereas the Euler model exhibits period-doubling and Neimark–Sacker bifurcations, as illustrated by the bifurcation diagram. This occurs because the stability of each fixed point in the Euler model depends on h, so variations in h affect their stability. In contrast, the stability of the fixed points in the NSFD model does not depend on the stepsize h, making it dimensionally consistent and not undergoing bifurcation. In addition to the issue of dynamic consistency, a case study on loan data has been performed using two performance metrics, R^2 and RMSE. Both models provide realistic parameter estimates and are capable of capturing the upward trend of the data. Based on the RMSE results, the NSFD model demonstrates better performance than the Euler model for each stepsize h.

This study reveals numerically the existence of period-doubling and Neimark–Sacker bifurcations. However, these bifurcations have not yet been shown analytically. For future work,

both bifurcations need to be demonstrated analytically to evaluate their bifurcation points. Furthermore, the maximum Lyapunov exponent can be provided to examine the stable, periodic, and chaotic conditions.

Author Contributions. **Raqqasyi Rahmatullah Musafir**: conceptualization, validation, formal analysis, investigation, writing—original draft preparation, writing—review and editing, supervision, project administration, funding acquisition. **Meylita Sari**: software, methodology, validation, writing—original draft preparation, writing—review and editing, visualization. These authors contributed equally to this work.

Acknowledgement. The authors are thankful the editors and reviewers who have supported us in improving this manuscript.

Funding. This research received no external funding.

Conflict of interest. The authors declare no conflict of interest.

Data availability. Not applicable.

References

[1] N. Sumarti, M. A. Aqsha, and M. F. Ansori, "Dynamic models of banking using a system of deterministic differential equations," *Available at SSRN 4213241*, 2023, doi: 10.2139/ssrn.4213241.

[2] M. F. Ansori, K. A. Sidarto, and N. Sumarti, "Model of deposit and loan of a bank using spiral optimization algorithm," *Journal of the Indonesian Mathematical Society*, vol. 25, no. 3, pp. 292–301, 2019, doi: 10.22342/jims.25.3.826.292-301.

[3] A. Fadhlurrahman and N. Sumarti, "Implementation of the dynamical system of the deposit and loan growth based on the lotka-volterra model and the improved model," in *AIP Conference Proceedings*, vol. 1723, no. 1. AIP Publishing LLC, 2016, p. 030007, doi: 10.1063/1.4945065.

[4] S. Arping, "Deposit competition and loan markets," *Journal of Banking & Finance*, vol. 80, pp. 108–118, 2017, doi: 10.1016/j.jbankfin.2017.04.006.

[5] R. R. Musafir, A. Suryanto, I. Darti *et al.*, "Optimal control of a fractional-order monkeypox epidemic model with vaccination and rodents culling," *Results in Control and Optimization*, vol. 14, p. 100381, 2024, doi: 10.1016/j.rico.2024.100381.

[6] G. Wang and A. Gunasekaran, "Modeling and analysis of sustainable supply chain dynamics," *Annals of Operations Research*, vol. 250, no. 2, pp. 521–536, 2017, doi: 10.1007/s10479-015-1860-2.

[7] M. Rayungsari, R. R. Musafir, and D. Savitri, "Dynamics of a fractional-order predator-prey model incorporating allee effect and cannibalism," in *AIP Conference Proceedings*, vol. 3302, no. 1. AIP Publishing LLC, 2025, p. 030002, doi: 10.1063/5.0261992.

[8] S. H. Strogatz, *Nonlinear dynamics and chaos with student solutions manual: With applications to physics, biology, chemistry, and engineering*. CRC press, 2018, doi: 10.1201/9780429399640.

[9] T. R. Malthus, *An Essay on the Principle of Population Or a View of Its Past and Present Effects on Human Happiness, an Inquiry Into Our Prospects Respecting the Future Removal Or Mitigation of the Evils which it Occasions by Rev. TR Malthus*. Reeves and Turner, 1872.

[10] N. Sumarti, R. Nurfitriyana, and W. Nurwenda, "A dynamical system of deposit and loan volumes based on the lotka-volterra model," in *AIP Conference Proceedings*, vol. 1587, no. 1. American Institute of Physics, 2014, pp. 92–94, doi: 10.1063/1.4866541.

[11] O. F. Damayanti, I. Darti, and A. Suryanto, "Dynamics of deposit and loan volumes model with non-performing loan and deposit withdrawal factors," *European Journal of Pure and Applied Mathematics*, vol. 18, no. 1, pp. 5643–5643, 2025, doi: 10.29020/nybg.ejpam.v18i1.5643.

[12] H. Ramanda, B. Handari, and D. Aldila, "Numerical simulation of stochastic model for deposit and loan volume based on the lotka-volterra model," in *AIP Conference Proceedings*, vol. 2023, no. 1. AIP Publishing LLC, 2018, p. 020216, doi: 10.1063/1.5064213.

[13] H. S. Panigoro, R. Resmawan, E. Rahmi, M. A. Beta, and A. T. R. Sidik, "The existence of a limit-cycle of a discrete-time lotka-volterra model with fear effect and linear harvesting," in *E3S Web of Conferences*, vol. 400. EDP Sciences, 2023, p. 03003, doi: 10.1051/e3sconf/202340003003.

[14] M. Rayungsari, A. Suryanto, W. Kusumawinahyu, and I. Darti, "Nonstandard numerical scheme for a predator-prey model involving predator cannibalism and refuge," *Communication in Biomathematical Sciences*, vol. 6, no. 1, pp. 11–23, 2023, doi: 10.5614/cbms.2023.6.1.2.

[15] R. E. Mickens, *Applications of nonstandard finite difference schemes*. World Scientific, 2000, doi: 10.1142/4272.

[16] A. Suryanto and I. Darti, "On the nonstandard numerical discretization of sir epidemic model with a saturated incidence rate and vaccination," *AIMS Math*, vol. 6, no. 1, pp. 141–155, 2021, doi: 10.3934/math.2021010.

[17] J. Pinto, S. Vaz, and D. F. Torres, "A lotka–volterra-type model analyzed through different techniques," in *Computational and Mathematical Models in Biology*. Springer, 2023, pp. 129–157, doi: 10.1007/978-3-031-42689-6_6.

[18] A. Vincent and N. Sumarti, "Implementation of the banking dynamics model using a system of deterministic differential equations," *Frontiers in Applied Mathematics and Statistics*, vol. 11, p. 1517447, 2025, doi: 10.3389/fams.2025.1517447.

[19] M. Monti, "Deposits, credit and interest rate determination under alternative bank objectives. szego, gp & shell, k. edition. mathematical methods in investment and finance," 1972.

[20] S. Elaydi, *An introduction to difference equations*. Springer, 2005, doi: 10.1007/0-387-27602-5.

[21] M. Martcheva, *An introduction to mathematical epidemiology*. Springer, 2015, vol. 61, doi: 10.1007/978-1-4899-7612-3.

[22] S. N. Elaydi, *Discrete chaos: with applications in science and engineering*. Chapman and Hall/CRC, 2007, doi: 10.1201/9781420011043.

[23] O. J. K. (OJK), "Portal ojk," https://ojk.go.id, 2025, accessed on 18 August 2025.